Electrical control of a solid-state flying qubit

Michihisa Yamamoto[1,2]*, Shintaro Takada[1], Christopher Bäuerle[1,3], Kenta Watanabe[1], Andreas D. Wieck[4] and Seigo Tarucha[1,5]

Solid-state approaches to quantum information technology are attractive because they are scalable. The coherent transport of quantum information over large distances is a requirement for any practical quantum computer and has been demonstrated by coupling super-conducting qubits to photons[1]. Single electrons have also been transferred between distant quantum dots in times shorter than their spin coherence time[2,3]. However, until now, there have been no demonstrations of scalable 'flying qubit' architectures—systems in which it is possible to perform quantum operations on qubits while they are being coherently transferred—in solid-state systems. These architectures allow for control over qubit separation and for non-local entanglement, which makes them more amenable to integration and scaling than static qubit approaches. Here, we report the transport and manipulation of qubits over distances of 6 μm within 40 ps, in an Aharonov–Bohm ring connected to two-channel wires that have a tunable tunnel coupling between channels. The flying qubit state is defined by the presence of a travelling electron in either channel of the wire, and can be controlled without a magnetic field. Our device has shorter quantum gates (<1 μm), longer coherence lengths (~86 μm at 70 mK) and higher operating frequencies (~100 GHz) than other solid-state implementations of flying qubits[4,5].

The flying qubit device described in this Letter is an electrical analogue of an optical two-path interferometer, in which the qubit basis is defined by the presence of a travelling electron in either of the two paths. Similar electrical two-path interference has been achieved in Mach–Zehnder interferometers of quantum Hall edge channels[4,5], which have been the testing grounds for quantum physics such as orbital entanglement[6,7]. However, these devices exhibit edge-channel coherence lengths of 24 μm at 20 mK (ref. 5). This, together with a requirement for high magnetic fields, limits their scalability.

Compared with edge-channel two-path interferometers, our two-path interferometer operates at a lower magnetic field, has well-defined quantum operations, shorter quantum gates and longer coherence lengths. Despite its apparent simplicity, the realization of such an electrical two-path interferometer at low magnetic fields is highly challenging. The main difficulty comes from the nature of the electrons on the Fermi surface—electrons usually take multiple paths, so the quantum phase of an electron is easily scrambled. This causes the quantum information being carried by the electron to be lost.

Electrons travelling through an Aharonov–Bohm (AB) interferometer[8–11], generally known as a two-path interferometer, also suffer from the existence of multiple paths. Electron interference arises in AB interferometers due to the phase the electron acquires in one path relative to the other, with the phase difference being given by $\Delta\varphi = \oint \mathbf{k} \cdot \mathbf{dl} - (e/\hbar)BS$. Here, B is the perpendicular magnetic field and S is the area enclosed by the AB ring. This phase difference causes an oscillation of the current as a function of B with a period of h/eS. It turns out, however, that the two-terminal linear conductance through an AB ring suffers from so-called phase rigidity[12–14]. Onsager's law for linear conductance[12,15,16], $G(B) = G(-B)$, implies that the phase of the AB oscillation can take only the values 0 or π at $B = 0$. To satisfy this boundary condition imposed by the contact geometry while still allowing for a continuous phase variation $\Delta\varphi$, contributions from multiple scattered paths need to be added to $\Delta\varphi$. What is usually observed in an AB experiment is therefore not an ideal two-path interference, but a complicated multipath interference. Such conventional AB interference is shown in Fig. 1b,c. Multi-terminal devices have also been used to extract the contribution of the two-path interference and avoid phase rigidity[17]. However, the multipath contribution is still present even in such interferometers, and leads to the loss of quantum information carried by coherent electrons reaching other reservoirs.

Here, we realize a novel two-path interferometer that can act as a flying qubit by combining the AB ring with two-channel wires, that is, parallel tunnel-coupled quantum wires[18,19] that allow tunnelling of an electron between the two paths (Fig. 1). We define the two pseudo spin states $|\uparrow\rangle$ and $|\downarrow\rangle$, where $|\uparrow\rangle$ and $|\downarrow\rangle$ correspond to the state having an electron in the upper and lower path, respectively[20–22]. In such a structure, any superposition state of $|\uparrow\rangle$ and $|\downarrow\rangle$ in the ring can transmit into the tunnel-coupled wire by being directly transformed into the superposition of the bonding and antibonding state in the tunnel-coupled wire, that is, $\psi_S = (1/\sqrt{2})(|\uparrow\rangle + |\downarrow\rangle)$ and $\psi_{AS} = (1/\sqrt{2})(|\uparrow\rangle - |\downarrow\rangle)$. This is in contrast with the conventional AB ring with only single wire leads, where only ψ_S is transmitted into the leads. Consequently, this new structure works as a two-path interferometer for ballistic electrons, which does not suffer from paths encircling the AB ring due to the absence of backscattering at the entrance of the tunnel-coupled wire. The pseudo spin is then defined as a flying qubit. It is important to mention that even though the electron wave spreads over the interferometer under low-energy excitation, the pseudo spin state is explicitly defined at each position in the interferometer (see Supplementary Information). Therefore, a flying qubit state carried by each single electron is strictly defined as a function of the position without uncertainty.

Our device (Fig. 1a) is defined by surface Schottky gates in a two-dimensional electron gas at the interface of a high-mobility GaAs/AlGaAs heterostructure. The negative gate voltages V_{T1} and V_{T2} applied on the orange-coloured central gates allow control of the tunnel coupling between the upper and lower paths. Because these gates are as narrow as 50 nm at the tunnel-coupled regions, the tunnel coupling at the right coupled wire can be kept sufficiently strong, even when the central region of the device is depleted by V_{T1} to form an AB ring. The side gates of the AB ring, V_{M1} and V_{M2},

[†]Department of Applied Physics, University of Tokyo, Bunkyo-ku, Tokyo, 113-8656, Japan, [2]ERATO-JST, Kawaguchi-shi, Saitama 331-0012, Japan, [3]Institut Néel – CNRS and Université Joseph Fourier, 38042 Grenoble, France, [4]Chair of Applied Solid-State Physics, Ruhr-Universität Bochum, D-44780 Bochum, Germany, [5]ICORP (International Cooperative Research Project) Quantum Spin Information Project, Atsugi-shi, Kanagawa, 243-0198, Japan. *e-mail: yamamoto@ap.t.u-tokyo.ac.jp
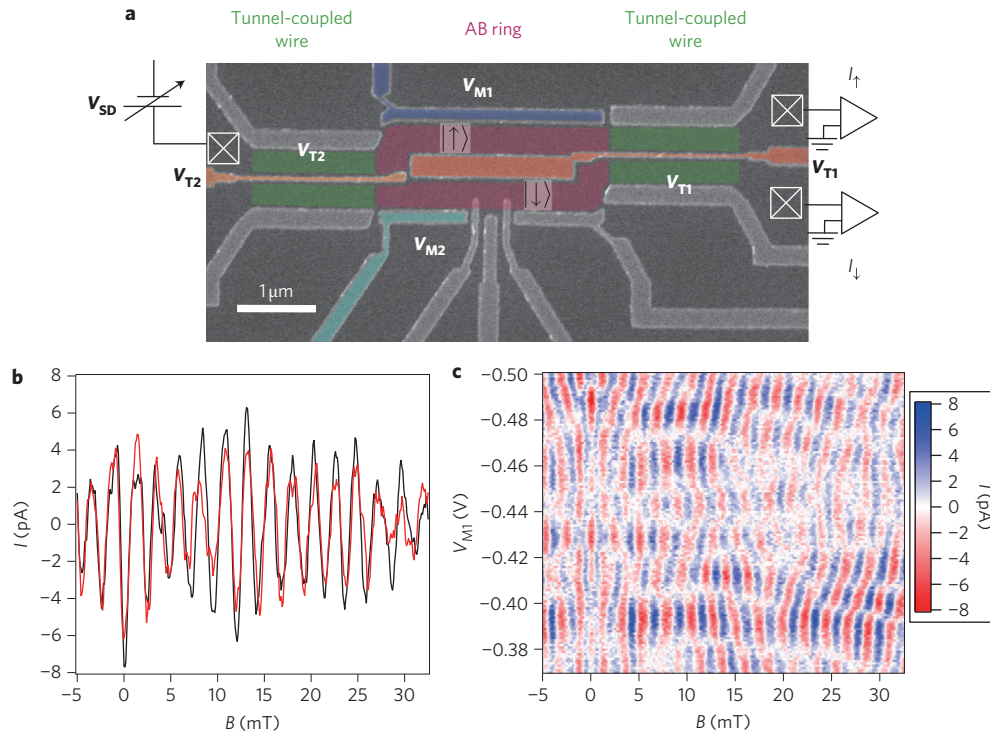
Figure 1 | Device image and observed conventional AB oscillation. a, Scanning electron microscopy image of the flying qubit device with a schematic of the experimental set-up. The device was defined by Schottky gates in an n-AlGaAs/GaAs 2DEG-based heterostructure (2DEG: $n = 1.9 \times 10^{11}$ cm^{-2}, $\mu \approx 2 \times 10^6$ cm^2 V^{-1} s^{-1}, depth = 125 nm) using standard split-gate techniques. The mean free path is 14.5 μm. V_{T1} and V_{T2} allow for control of tunnel coupling between the parallel quantum wires, and V_{M1} and V_{M2} modify the Fermi wave vector at each path. Three 'cross-in-square' symbols represent ohmic contacts. **b**, Typical AB oscillation measured at $T = 70$ mK for $V_{T2} = 0$ and $V_{M1} = -0.391$ V. Black and red curves are currents $I_\uparrow$ and $I_\downarrow$, obtained at the upper and the lower contacts, respectively. Negative gate voltage V_{T1} is set to be low enough ($V_{T1} = -0.300$ V) that the propagating electrons do not occupy the antisymmetric orbital in the right tunnel-coupled wire. This three-terminal device then effectively works as a two-terminal device, resulting in a similar oscillation between $I_\uparrow$ and $I_\downarrow$. The oscillation components are extracted by subtracting a smoothed background. **c**, Intensity plot of $I_\uparrow$ as a function of the perpendicular magnetic field and V_{M1}. Owing to phase rigidity, the phase at $B = 0$ is either 0 or π. Sweeping V_{M1}, many π jumps are observed in the phase, which occur due to the multipath interference.

allow modulation of the Fermi wave vectors in the ring. All measurements except those in Figs 2 and 4 were carried out in a dilution refrigerator at 70 mK.

The initial qubit state is simply defined as $|\uparrow\rangle$ by injecting electrons into only one of the two wires. The projection of the final state is obtained by measuring the output currents, $I_\uparrow$ and $I_\downarrow$. Tunnel coupling between the two wires yields the hybridized symmetric and antisymmetric basis states, ψ_S and ψ_{AS}, with confinement energies E_S and E_{AS}, respectively. The energy spacing $\Delta E = E_{AS} - E_S$ is given by the tunnel coupling energy. The quantum state of an electron wave, which is a superposition state of ψ_S and ψ_{AS}, then acquires a relative phase $\theta = (1/\hbar)\Delta E \tau$ between ψ_S and ψ_{AS}, where $\tau \approx L_t/v_F$ is the traversal time for electrons propagating over the length L_t of the tunnel coupling with Fermi velocity v_F. θ is the rotation angle of a state vector about the x-axis on the Bloch sphere (see Supplementary Information). This rotational operator is expressed as the matrix

$$R_x(\theta) = \begin{pmatrix} \cos\dfrac{\theta}{2} & i\sin\dfrac{\theta}{2} \\ i\sin\dfrac{\theta}{2} & \cos\dfrac{\theta}{2} \end{pmatrix}$$

It follows that if an electron is injected into one of the wires, the pseudo spin state at the end of the tunnel-coupled wire periodically oscillates between $|\uparrow\rangle$ and $|\downarrow\rangle$ as a function of the tunnel coupling energy due to this rotational operation.

We demonstrated $R_x(\theta)$ by depleting the region beneath gate V_{T2}. A current was injected into one of the wires and measured via output currents $I_\uparrow$ and $I_\downarrow$ as a function of gate voltage V_{T1}. Evolution of the pseudo spin state of an electron propagating through the tunnel-coupled wire is schematically depicted in Fig. 2a, where the rotation angle θ depends on V_{T1}. Clear antiphase oscillations of currents $I_\uparrow$ and $I_\downarrow$ were observed at 2.2 K, as shown in Fig. 2b,c, which cancel each other in the total current $I_\uparrow + I_\downarrow$. The total current has only a weak dependence on V_{T1}. This means that there is basically no backscattering for the oscillating signal transmitted through the tunnel-coupled wire. The antiphase oscillations are therefore evidence of the oscillation of the electron between the two wires, induced by tunnel coupling. Here the visibility of the oscillation, the ratio of the oscillation component to the total current, is limited to ~1%. This is due to the existence of a few transmitting channels and the high measurement temperature (see Supplementary Information). Note that at low temperatures, disorder scattering in the quantum wires leads to complicated fluctuations of the output currents as a function of V_{T1}, which masks the current oscillation induced by tunnel coupling.

A rotation about the z-axis can be achieved in the AB ring by varying the magnetic field or the gate voltages V_{M1} and V_{M2}. The relative transmission phase φ between $|\uparrow\rangle$ and $|\downarrow\rangle$ is given by

$$\varphi = \int_P^Q \left(\mathbf{k} - \frac{e}{\hbar}\mathbf{A}\right) \cdot d\mathbf{l}_\downarrow - \int_P^Q \left(\mathbf{k} - \frac{e}{\hbar}\mathbf{A}\right) \cdot d\mathbf{l}_\uparrow = \oint \mathbf{k} \cdot d\mathbf{l} - \frac{e}{\hbar}BS$$
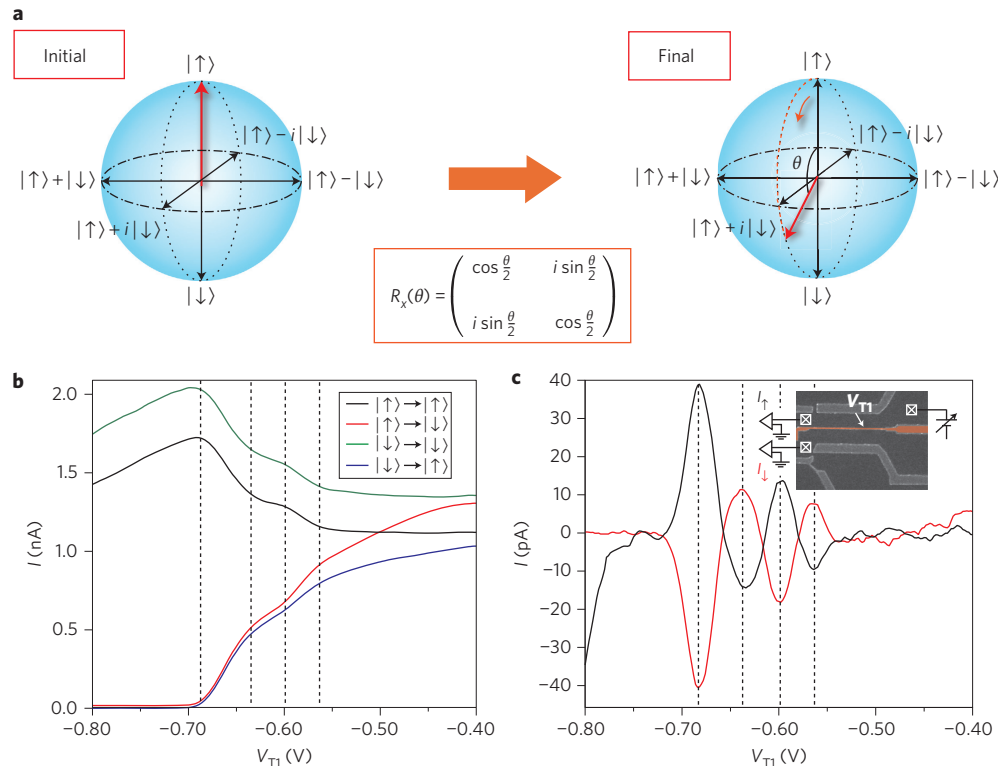
Figure 2 | Demonstration of R_x operation. a, Evolution of the flying charge qubit state via tunnel coupling. **b**, Measured output currents in the tunnel-coupled wire. There are at least three transmitting modes in each wire (see Supplementary Information). Black and red curves are the output currents $I_\uparrow$ and $I_\downarrow$ measured as a function of gate voltage V_{T1} for $V_{sd} = 50\,\mu V$, $V_{T2} = -0.84\,V$ and $T = 2.2\,K$ when the current is injected from the upper wire. Blue and green curves are measured output currents $I_\uparrow$ and $I_\downarrow$ when the current is injected to the lower wire with the same gate voltage configuration. Coincidences between the black and green curves and between the red and blue curves indicate that the oscillation of the current is due to tunnel coupling between the two paths. Note that the measurement of the current at such a high T does not suffer from universal conductance fluctuations originating from disorder. **c**, Oscillating component of the output currents. Smoothed backgrounds are subtracted from the black and red curves of **b**.
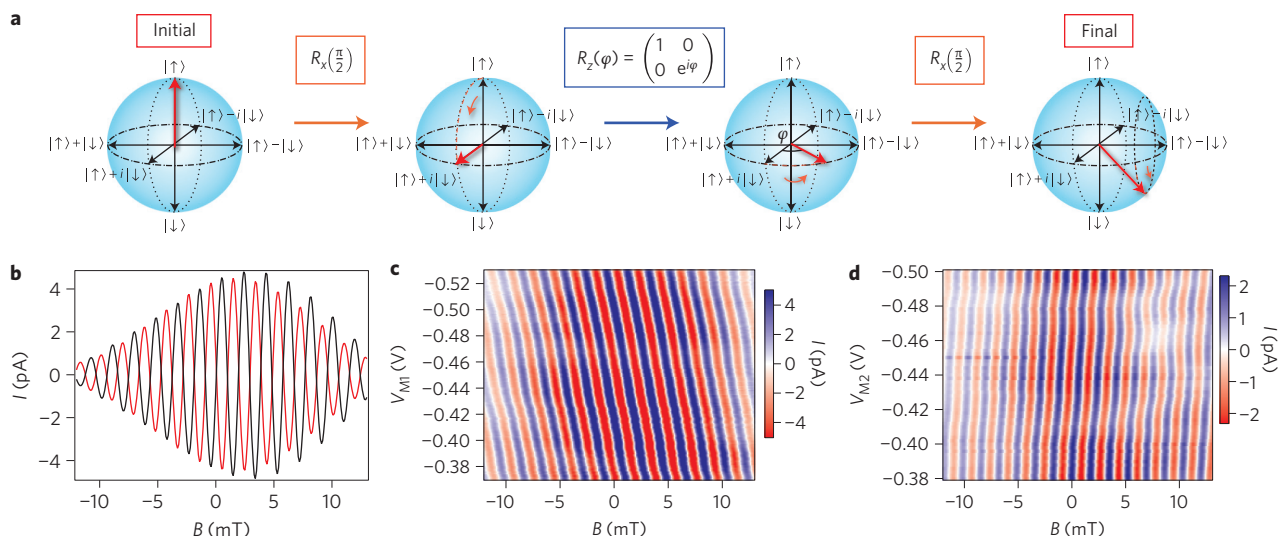

Figure 3 | Demonstration of R_z operation. a, Evolution of the flying qubit state in the scheme of Ramsey interference. **b**, Output current oscillation as a function of magnetic field. Black and red curves are output currents $I_\uparrow$ and $I_\downarrow$, respectively, measured for $V_{sd} = 50\,\mu V$. Both tunnel-coupled wires work as $R_x(\pi/2)$, which results in maximum current oscillation (see Supplementary Information). **c**, Intensity plot of $I_\uparrow$ as a function of magnetic field B and side gate voltage V_{M1}. **d**, Intensity plot of $I_\uparrow$ as a function of B and V_{M2}. The oscillation components are extracted by a Hamming window followed by a fast Fourier transform filter for **b–d**. In both **c** and **d**, there is no phase jump of π, in contrast to Fig. 1c, which is a proof of the two-path interference. The smooth phase shift is given by $\Delta\varphi = \Delta k_F \cdot L_i = (\pi C_i L_i / 2e)\Delta V_{Mi}$, where $L_{1(2)}$ is the length of the upper (lower) path and $C_{1(2)}$ is the capacitance per length between the gate and the upper (lower) quantum wire. We obtained $C_1 \approx C_2 \approx 2.9\,pF\,m^{-1}$ from the data in **c** and **d**.
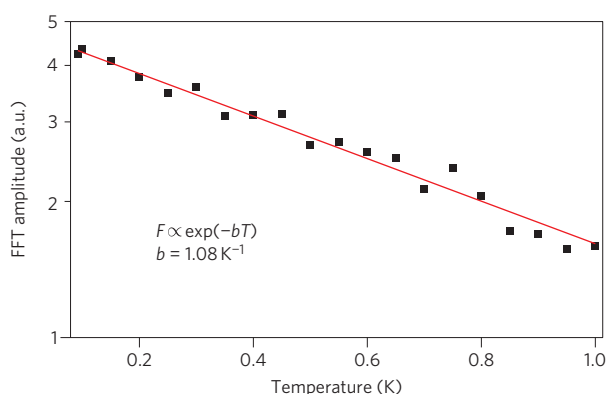
Figure 4 | Evaluation of coherence length l_φ. Temperature dependence of the fast Fourier transform (FFT) amplitude, F. The exponential decay suggests that the decoherence rate is proportional to T and therefore $l_\varphi \propto 1/T$ assuming v_F is constant. We obtained the slope of 1.08 K^{-1} by fitting the data (red line). Considering that the length of the interferometer is 6.5 µm, we set $l_\varphi = 6.5$ µm at $T = 1/1.08$ K$^{-1} = 0.93$ K. With $l_\varphi \propto 1/T$, we estimate $l_\varphi \approx 86$ µm at $T = 70$ mK.

(where P and Q are the positions where the wave splits and recombines, respectively) and is defined as a rotation angle for the rotational operator about the z-axis on the Bloch sphere:

$$R_z(\varphi) = \begin{pmatrix} 1 & 0 \\ 0 & e^{i\varphi} \end{pmatrix}$$

The combination of R_x and R_z enables the generation of an arbitrary vector state on the Bloch sphere. Arbitrary rotation of the state is also possible by simultaneously controlling the tunnel coupling and the difference of the transmission phase between the two paths.

$R_z(\varphi)$ was demonstrated in the scheme of a Ramsey interference (Fig. 3a) using a high-velocity channel that is insensitive to the disorder. We established the two sets of tunnel-coupled wires to prepare $R_x(\pi/2)$ (see Supplementary Information) and varied the magnetic field to prepare $R_z(\varphi)$ in the AB ring. The measured $I_\uparrow$ and $I_\downarrow$ plotted in Fig. 3b show AB oscillations with exactly opposite phases, indicating that the two-path interference is dominant over the multipath contributions of backscattering. The difference in amplitude between $I_\uparrow$ and $I_\downarrow$ is the backscattered term and is much smaller than the main oscillation.

To further confirm the two-path interference and electrical control of the qubit, we also swept the gate voltages V_{M1} and V_{M2} to modulate the Fermi wave vector k_F of the respective paths, as shown in Fig. 3c,d. The phase evolves almost linearly and smoothly over 2π with the gate voltages, in strong contrast to Fig. 1c. These results therefore demonstrate ideal two-path interference with no phase rigidity, and the qubit can be controlled even without a magnetic field.

The flying qubit presented here is promising for quantum information technology. In addition to the ability to transfer the quantum information over a long distance, it has a much shorter operation time compared with other qubits in solid-state systems. The operation time L/v_F (L, gate length; v_F, Fermi velocity) is of the order of 10 ps (see Supplementary Information). We also found, by analysing the temperature dependence of the oscillation amplitude (Fig. 4), that this qubit has a very long coherence length l_φ. Assuming that the electron travels with constant velocity, the exponential decay of the amplitude[23–26] (as observed in Fig. 4) leads to the relationship $l_\varphi \propto 1/T$. We obtained $l_\varphi = 86$ µm at 70 mK from the decaying rate (see Fig. 4 caption). This value is much larger than that reported for a Mach–Zehnder interferometer

of an edge state[5], in which limited coupling between the interferometer and the reservoir via only a few edge channels makes the interferometer sensitive to charge fluctuation[23].

The only drawback of the present arrangement is the limited visibility, defined as the AB oscillation amplitude divided by the total current, which is only ~0.3% for the measurements of Fig. 3b–d (see Supplementary Information). Because the coherence length is found to be much longer than the interferometer length, decoherence is not the origin of this low visibility. The influence of thermal smearing due to the difference in Fermi velocity between the two paths is also small at our measurement temperature (see Supplementary Information). The visibility should be improved by optimizing the device design; for example, there are two possible 'geometrical' reasons for the low visibility. First, the entrance and exit of the tunnel-coupled wires are so narrow that the conductance may be restricted there and backscattering may occur. Second, there is a contribution from several transmitting channels in each part of the tunnel-coupled wires and in each arm of the AB ring, although only one in each wire contributes to the main oscillation. A possible remedy is to make use of a high-electron-density heterostructure to define strongly confined single-mode channels, and to make the electrons propagate through them without suffering from backscattering. Indeed, we have significantly improved the visibility to ~10% by using a high-electron-density heterostructure and by defining narrower channels (see Supplementary Information).

In addition to the quantum information transfer, it should also be possible to create a non-local entanglement state following the scheme proposed in refs 21 and 22, combined with single electron sources[27,28] to synchronize qubits. This flying qubit can also be used in combination with a static qubit[29]. Using a high-mobility heterostructure with a mean free path exceeding 100 µm, we would in principle be able to integrate 100 qubits because each quantum operation, including two-qubit operation, is performed within a 1 µm scale (see Supplementary Information).

References

1. Wallraff, A. *et al.* Strong coupling of a single photon to a superconducting qubit using circuit quantum electrodynamics. *Nature* **431,** 162–167 (2004).
2. Hermelin, S. *et al.* Electrons surfing on a sound wave as a platform for quantum optics with flying electrons. *Nature* **477,** 435–438 (2011).
3. McNeil, R. *et al.* On-demand single-electron transfer between distant quantum dots. *Nature* **477,** 439–442 (2011).
4. Ji, Y. *et al.* An electronic Mach–Zehnder interferometer. *Nature* **422,** 415–418 (2003).
5. Roulleau, P. *et al.* Direct measurement of the coherence length of edge states in the integer quantum Hall regime. *Phys. Rev. Lett.* **100,** 126802 (2008).
6. Samuelsson, P., Sukhorukov, E. V. & Büttiker, M. Two-particle Aharonov–Bohm effect and entanglement in the electronic Hanbury Brown–Twiss setup. *Phys. Rev. Lett.* **92,** 026805 (2004).
7. Neder, I. *et al.* Interference between two indistinguishable electrons from independent sources. *Nature* **448,** 333–337 (2007).
8. Aharonov, Y. & Bohm, D. Significance of electromagnetic potentials in the quantum theory. *Phys. Rev.* **115,** 485–491 (1949).
9. Washburn, B. S. & Webb, R. A. Aharonov–Bohm effect in normal metal quantum coherence and transport. *Adv. Phys.* **35,** 375–422 (1986).
10. Tonomura, A. *et al.* Observation of Aharonov–Bohm effect by electron holography. *Phys. Rev. Lett.* **48,** 1443–1446 (1982).
11. Giesbers, A. J. M. *et al.* Correlation-induced single-flux-quantum penetration in quantum rings. *Nature Phys.* **6,** 173–177 (2010).
12. Onsager, L. Reciprocal relations in irreversible process. *Phys. Rev.* **38,** 2265–2279 (1931).
13. Yeyati, A. L. & Büttiker, M. Aharonov–Bohm oscillations in a mesoscopic ring with a quantum dot. *Phys. Rev. B* **52,** R14360–R14363 (1995).
14. Yacoby, A., Schuster, R. & Heiblum, M. Phase rigidity and *h/2e* oscillations in a single-ring Aharonov–Bohm experiment. *Phys. Rev. B* **53,** 9583–9586 (1996).
15. Büttiker, M. Four-terminal phase-coherent conductance. *Phys. Rev. Lett.* **57,** 1761–1764 (1986).

16. Benoit, A. D., Washburn, S., Umbach, C. P., Laibowitz, R. B. & Webb, R. A. Asymmetry in the magnetoconductance of metal wires and loops. *Phys. Rev. Lett.* **57,** 1765–1768 (1986).
17. Schuster, R. *et al.* Phase measurement in a quantum dot via a double-slit interference experiment. *Nature* **385,** 417–420 (1997).
18. Del Alamo, J. A. & Eugster, C. C. Quantum field-effect directional coupler. *Appl. Phys. Lett.* **56,** 78–80 (1990).
19. Tsukada, N., Wieck, A. D. & Ploog, K. Proposal of novel electron wave coupled devices. *Appl. Phys. Lett.* **56,** 2527–2529 (1990).
20. Bertoni, A., Bordone, P., Brunetti, R., Jacoboni, C. & Reggiani, S. Quantum logic gates based on coherent electron transport in quantum wires. *Phys. Rev. Lett.* **84,** 5912–5915 (2000).
21. Ionicioiu, R., Zanardi, P. & Rossi, F. Testing Bell's inequality with ballistic electrons in semiconductors. *Phys. Rev. A* **63,** 050101(R) (2001).
22. Yu, L. & Voskoboynikov, O. Ballistic Aharonov–Bohm quantum bits and quantum gates. *Solid State Commun.* **145,** 447–450 (2008).
23. Seelig, G. & Büttiker, M. Charge-fluctuation-induced dephasing in a gated mesoscopic interferometer. *Phys. Rev. B* **64,** 245313 (2003).
24. Hansen, A. E., Kristensen, A., Pedersen, S., Sørensen, C. B. & Lindelof, P. E. Mesoscopic decoherence in Aharonov–Bohm rings. *Phys. Rev. B* **64,** 045327 (2001).
25. Kobayashi, K., Aikawa, H., Katsumoto, S. & Iye, Y. Probe-configuration-dependent decoherence in an Aharonov–Bohm ring. *J. Phys. Soc. Jpn* **71,** 2094–2097 (2002).
26. Seelig, G., Pilgram, S., Jordan, A. N. & Büttiker, M. Probe-configuration-dependent dephasing in a mesoscopic interferometer. *Phys. Rev. B* **68,** 161310(R) (2003).
27. Blumenthal, M. D. *et al*. Gigahertz quantized charge pumping. *Nature Phys.* **3,** 343–347 (2007).
28. Fève, G. *et al*. An on-demand coherent single-electron source. *Science* **316,** 1169–1172 (2007).
29. Schomerus, H. & Robinson, J. P. Entanglement between static and flying qubits in an Aharonov–Bohm double electrometer. *New J. Phys.* **9,** 67 (2007).

Author contributions

M.Y. conceived the experiments, performed part of the experiments, interpreted the data and wrote the manuscript with C.B. and S. Tarucha. S. Takada fabricated the samples and conducted measurements and analysis. C.B. contributed to the experimental set-up and interpretation of the data. K.W. performed the experiments on decoherence with S. Takada. S. Takada, K.W. and C.B. carried out the high visibility measurements in Grenoble as presented in the Supplementary Information. A.D.W. provided the high-mobility heterostructures. S. Tarucha directed the research. All authors discussed the results and the manuscript extensively.

Additional information

The authors declare no competing financial interests. Supplementary information accompanies this paper at www.nature.com/naturenanotechnology. Reprints and permission information is available online at http://www.nature.com/reprints. Correspondence and requests for materials should be addressed to M.Y.